Energy & Environmental Science

RSC Publishing

PAPER

View Article Online
View Journal | View Issue

Cite this: *Energy Environ. Sci.*, 2013, **6**, 2756

On the role of intermixed phases in organic photovoltaic blends†

Paul Westacott,[ab] John R. Tumbleston,[c] Safa Shoaee,[bd] Sarah Fearn,[a] James H. Bannock,[bd] James B. Gilchrist,[ab] Sandrine Heutz,[ab] John deMello,[bd] Martin Heeney,[bd] Harald Ade,[c] James Durrant,[bd] David S. McPhail[a] and Natalie Stingelin*[ab]

Received 28th May 2013
Accepted 23rd July 2013

DOI: 10.1039/c3ee41821a

www.rsc.org/ees

Recently, an intermixed phase has been identified within organic photovoltaic (OPV) bulk heterojunction (BHJ) systems that can exist in addition to relatively phase-pure regions, highlighting the need for a refined picture of the solid-state microstructure of donor–acceptor blends and for gaining further understanding of the exact nature and role such intermixed phases play in such devices. Here we manipulate the microstructure of polymer–fullerene systems *via* processing means and the selection of the molecular weight of the donor polymer. This manipulation is used as a tool to vary the fraction of intermixed phase present and its effects on the structure and subsequently the opto-electronic processes. We find clear relationships between the state of mixing and amount of exciton quenching and number of polarons generated per absorbed photon. Furthermore, we observe that blend systems incorporating higher molecular weight polymer result in a greater yield of dissociated polarons, likely due to the increase of the intermixed fraction.

Broader context

Photovoltaics (PV) hold tremendous potential as a technology to address the rising global demand for clean energy. One key for wide-spread success of this technology is to drive down the cost per Watt of electricity. This requires utilisation of less energy-intensive/lower cost production methods. One highly promising emerging technology for this is organic photovoltaics (OPVs). OPVs promise large-area manufacturing of future products by high-throughput roll-to-roll processing in ambient conditions. OPVs have also seen a rapid improvement in performance over recent years with certified devices reaching 10% power conversion efficiency. However there still remain fundamental questions related to the exact microstructure that needs to be realised within the active layer of such solar cells to optimise – and further improve – their power conversion efficiency. A structural picture is also necessary to target specific processing protocols and permit reliable device fabrication at high yield. The active layer of bulk-heterojunction (BHJ) OPVs is comprised of a blend of an electron-donating and an electron-accepting material, which until recently were generally believed to form relatively pure phases. However new studies have indicated that the BHJ microstructure may also contain a phase, where both materials can be mixed at much more intimate scales. In this paper, we discuss the role of this intermixed phase. We propose a strong influence of the presence of such an intermixed phase on the opto-electronic processes of the system and provide structural guidelines for further improving the efficiency of BHJ OPVs.

Organic photovoltaics (OPVs) consisting of a semiconducting polymer and a fullerene, blended into a bulk heterojunction (BHJ), offer great potential for high-throughput processing and promise to drastically lower material costs when compared to many of their inorganic counterparts. Over the last few years, there has been phenomenal improvement in the power conversion efficiency (PCE) within the OPV field due to increased commercial and academic interest, resulting in devices with certified efficiencies of 10%.[1] Nonetheless, there still remains a significant challenge in understanding the complex microstructure that is formed upon deposition of the donor:acceptor blend and how this is related to the series of processes that lead to maximum photocurrent.

The rapid enhancement of PCE of OPVs in recent years has been in large part due to the wide range of novel polymers that have been developed, many of which consist of "push–pull" alternating monomer units.[2–6] These new materials have, however, been reported to form a variety of microstructures and can require widely different processing protocols with respect to selection of solvents and blend composition, use of additives, specific thermal treatments,[7,8] *etc.*, in order to produce efficient devices. For every newly developed material system, intricate

[a]*Department of Materials, Imperial College London, London, UK. E-mail: natalie.stingelin@imperial.ac.uk*
[b]*Centre for Plastic Electronics, Imperial College London, London, UK*
[c]*Department of Physics, North Carolina State University, Raleigh, NC, USA*
[d]*Department of Chemistry, Imperial College London, London, UK*

† Electronic supplementary information (ESI) available. See DOI: 10.1039/c3ee41821a

trial-and-error procedures are required to optimise OPV performance. For this reason enhancing the understanding of the interplay between desirable microstructural characteristics and the opto-electronic processes is vital for creating a platform that allows designing from the outset strategies of how to process such a diverse range of materials into efficient cells.

Establishment of relevant structure/processing/property interrelationships is rendered complex by the fact that recent work indicates that not only the crystalline fractions in organic donor:acceptor blends may play an important role with respect to their OPV performance, but also their less ordered phases where a more pronounced intermixing of the components can be expected[9–23] (leading in most cases to amorphous solid solutions of the two components). For example Pfannmöller *et al.*, observed within the BHJ of poly(3-hexylthiophene-2,5-diyl) (P3HT):phenyl-C_{61}-butyric acid methyl ester (PCBM) system,[9] using analytical electron microscopy, the presence of an intermixed phase in addition to the relatively pure phases formed by the two components (*i.e.* P3HT and PCBM). Furthermore work by Treat *et al.*, assessed the temperature dependence of mixing of different fullerenes into the amorphous phase of different semi-crystalline semiconducting polymers;[10,11] while Collins *et al.* and Watts *et al.* convincingly showed that at quasi-thermodynamic equilibrium, there is still a significant amount of fullerene intermixed within the polymer, implying the persistent presence of this amorphous solid solution.[12,13] Other work[14–23] further confirms the presence of such an additional phase in a range of polymer:fullerene systems with possible implications on how we describe the photophysical processes in such systems.

Conventionally, charge generation in OPVs has been considered to occur *via* photon absorption in a neat phase of one of the two active components, leading to the generation of an exciton which migrates to an interface between relatively phase-pure donor and acceptor domains within the BHJ structure before undergoing exciton dissociation over one or more steps that can lead to the generation of free charges.[24] However, in light of the recent reports of the presence of a finely intermixed phase which can comprise a significant fraction of the BHJ structures and other reports of ultrafast charge generation (<200 fs) in different polymer:fullerene systems,[25–29] the question might be raised whether the intermixed phase also contributes to charge generation. For instance, Troshin *et al.* found a strong correlation between the relative solubilities of the two components and the OPV performance of the corresponding BHJ film.[30] This is in agreement with more recent work by Treat *et al.*, who studied the miscibility of different fullerene derivatives in a semi-crystalline donor polymer and the effects on phase separation and device performance.[11] Moreover, the Siebbles research group observed that the charge generation in P3HT:PCBM could occur on ultrafast timescales and hence postulated that such processes may take place *via* a more direct route than described by the conventional model.[25] Clearly, subtly differing or competing processes will play a role in photogeneration depending on the phase morphology of the active layer, but there remains significant uncertainty about which features of the active layers' microstructure and phase morphology govern charge generation within BHJ systems and this raises interesting questions regarding our current conception of an "ideal" microstructure for OPV devices.

The phase morphology (*e.g.*, two-phase structure comprised of relatively pure phases *vs.* three phase morphology that comprises also an intermixed phase) that is formed by the active layer of a BHJ will depend on various parameters, including the miscibility of the two components and the processing routes selected to deposit the BHJ. These effects can be expected to be particularly relevant for some of the more recent, non-crystalline donor materials where the phase purity of this component can no longer be governed by crystallisation. Nonetheless, we discuss here the relatively crystalline P3HT:PCBM blend as a model system. This prototypical OPV binary has been shown to often exhibit a three-phase microstructure.[9,10,12] We selected P3HT of two different weight-average molecular weights (M_w)[31] to provide an additional tool to manipulate the phases that may be present in such blends *via* the length of the donor polymer chains, in analogy to cross-linked polymer:diluent systems where the molecular weight of the polymer has been observed to play a large role in the mixing behaviour.[32] The semi-crystalline nature of both components should offer further freedom in varying the relative fraction of phases present. An additional benefit of using P3HT as a donor polymer is that its steady state UV-vis absorption is much more sensitive to the local environment (*e.g.* backbone planarity, polymer aggregation) than many other materials, which can allow more localised insight into the molecular surroundings of this polymer. It is noted here that aggregation can occur in both crystalline and non-crystalline fractions of the material, as the ordering required to observe spectroscopic changes can be much more localised than the long range order expected from a crystal lattice.

The P3HTs of our choice were a material of low M_w (denoted in the following: "L-P3HT", $M_w = 7.2$ kg mol^{-1}) which forms a chain-extended microstructure,[33–35] and a high molecular-weight P3HT ("H-P3HT", $M_w = 135$ kg mol^{-1}) which will solidify in a semi-crystalline, two-phase (amorphous/crystalline) microstructure[33–35] upon typical solution processing. Indeed, the H-P3HT will be comprised of a significant portion of amorphous material with tie molecules, entanglements and loops (see schematic inset Fig. 1) capable of readily incorporating fullerene molecules to form an intermixed phase. We also varied the fullerene content, and produced blends of two compositions (*i.e.* 5 and 50 wt%) for both the L-P3HT and H-P3HT; the blends of a lower PCBM fractions will be in the dilute regime,[36] where we may expect a considerable fraction of the fullerene to be fully miscible with the P3HT without significantly altering the polymer microstructure. In contrast, at higher PCBM loading, the fullerene is likely to affect the ordering/aggregation of the polymer.[36,37] Note also that the most efficient devices have been reported for blends comprising around 50 wt% PCBM.[36,37]

We probed the charge generation yield of the various P3HT:PCBM systems by transient absorption spectroscopy (TAS). TAS measures the yield and decay dynamics of the dissociated polarons in these blend systems. The decay dynamics are indicative of the rate of non-geminate recombination, whilst the initial amplitude (ΔOD) is indicative of the initial yield of dissociated charges, attributed to dissociated

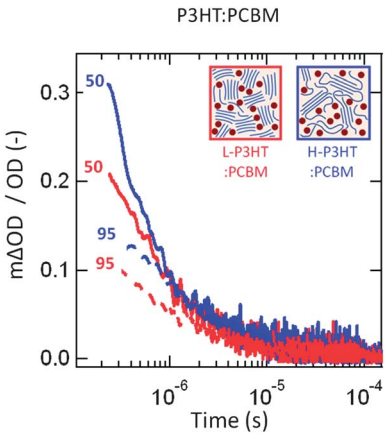

Fig. 1 Molecular weight dependence of dissociated polaron yield (ΔOD) of P3HT:PCBM binary blend films. Transient absorption yield and decay dynamics displaying the photo-induced absorption of $P3HT^+$ polarons (980 nm), following pulsed laser excitation (520 nm). A comparison is shown between P3HT:PCBM blends comprising P3HT of different molecular weight: $M_w = 7$ kg mol^{-1} (red) and $M_w = 135$ kg mol^{-1} (blue). The P3HT fraction (wt%) is also given. The blends were co-deposited from chlorobenzene (2% (w/v)). Inset: schematics depicting the proposed microstructure of L-P3HT:PCBM (left) and H-P3HT:PCBM (right) blends.

polarons. The yield of dissociated polarons is proportional to the observed ΔOD, given that for the same material system, the extinction coefficient of the probed species remains constant.[38] Furthermore, it has been shown previously that, for systems comprising P3HT:PCBM, the ΔOD correlates strongly with the short circuit current (J_{sc}) of devices and hence the ΔOD can be used as a convenient tool to investigate photo-physical processes that are relevant to devices.[39]

Micro-second-transient absorption studies of films were carried out at low-intensity (<4 μJ cm^{-2}) excitation conditions and data was generated at a probe wavelength of 980 nm corresponding to polymer positive polarons ($P3HT^+$).[40] All transients exhibited power law ($\Delta OD \propto t^{-a}$) and oxygen-independent decay dynamics, consistent with their assignment to polaron rather than triplet absorption. Whilst similar decay dynamics were observed for all films noticeable differences in dissociated polaron yield (ΔOD) were found between blends comprising H-P3HT and L-P3HT, respectively (Fig. 1). The H-P3HT:PCBM systems consistently exhibited a considerably larger ΔOD – around 30% (at 400 ns) higher for the binaries comprising 50 wt% P3HT. Similarly, at a P3HT content of 95 wt%, the ΔOD (at 400 ns) is approximately 40% higher for the H-P3HT:PCBM blend when compared to L-P3HT:PCBM. This corresponds to a 30–40% higher yield of dissociated polarons. At higher PCBM content, higher ΔOD are measured compared to the binaries comprising 95 wt% P3HT, consistent with a recent hypothesis that the PCBM aggregation, which generally occurs at this composition, is a key driver of charge separation in such systems.[41] Moreover, the amplitudes of observed decay transients varied approximately linearly with excitation density, and the decay dynamics of the dissociated polaron absorption for all the blend films were very similar, indicating that neither saturation effects nor non-geminate losses prior 200 ns significantly distorted this comparison.

The question arises why we see such differences in the ΔOD of the various P3HT:PCBM blends and how these relate to the different phase morphologies we expect to form in the four binaries. We, therefore, attempted to quantify the temperature-dependant miscibility of the fullerene in the two P3HTs[10] as a tool to try to understand and quantify the composition of the intermixed phase. For this purpose, we conducted dynamic secondary ion mass spectrometry (d-SIMS) and followed procedures established by Treat *et al.*[10] This required fabrication of bilayers of the polymer/fullerene systems through lamination, followed by an annealing procedure to drive the interdiffusion of the deuterated PCBM into the P3HT layer, rather than deposition of the two components from a common solvent as used for the sample preparation for TAS.[10]

First we scrutinised whether clean bilayers had been obtained by the lamination process. Sharp interfaces and distinct layers were indeed observed in high angle annular dark field scanning transmission electron microscopy (HAADF STEM) (Fig. 2B, top), implying that no significant intermixing had occurred during the fabrication of the bilayer (high resolution images are shown in Fig. S3†). This was confirmed by SIMS, where distinct layers of each material were observed. A more detailed discussion and interpretation of the data is provided in the ESI.†

In agreement with Treat *et al.*,[10] after only a short annealing step (30 s) at 150 °C, a considerably enhanced PCBM signal was observed in the previous, relatively phase-pure polymer layer (Fig. 2A bottom panels), implying a large degree of vertical mixing of the two components and a diffusion equilibrium. Further detailed discussion of these systems is presented in the ESI.† The effect of annealing produced moreover a noticeable loss of the compositional contrast between the P3HT and PCBM layers, as shown in HAADF STEM (Fig. 2B, bottom panel) suggesting that the two components interdiffused. These observations are a clear indication of a certain degree of miscibility between the donor and acceptor material (Fig. 2B). Surprisingly, especially when considering the large differences observed in TAS for H-P3HT:PCBM and L-P3HT:PCBM blends, no significant variation was found in the temperature-dependent intermixing between P3HT/PCBM bilayers comprising P3HT of different M_w (Fig. 2C) after annealing.

Does our d-SIMS data imply that there is no correlation between miscibility and charge generation? It may, but a number of other possibilities could also explain the fact that different ΔOD values are measured in TAS while similar PCBM:P3HT miscibility are found in d-SIMS, including: differences in the distribution of the PCBM or P3HT fraction within the various blend structures (*e.g.*, domain size or shape); kinetic effects of crystallisation related to the M_w of the polymer; or differences in the vitrification effect of the PCBM, to name a few. A further possibility is that the different processing routes, *i.e.* deposition from a co-solvent for the fabrication of thin blend films (as used for TAS measurements) *vs.* preparation of neat layers that are laminated into bilayers followed by solid-sate mixing through interdiffusion of the fullerene (as used for the d-SIMS analysis), could lead to different thin-film microstructures in such binaries, not allowing a straight-forward

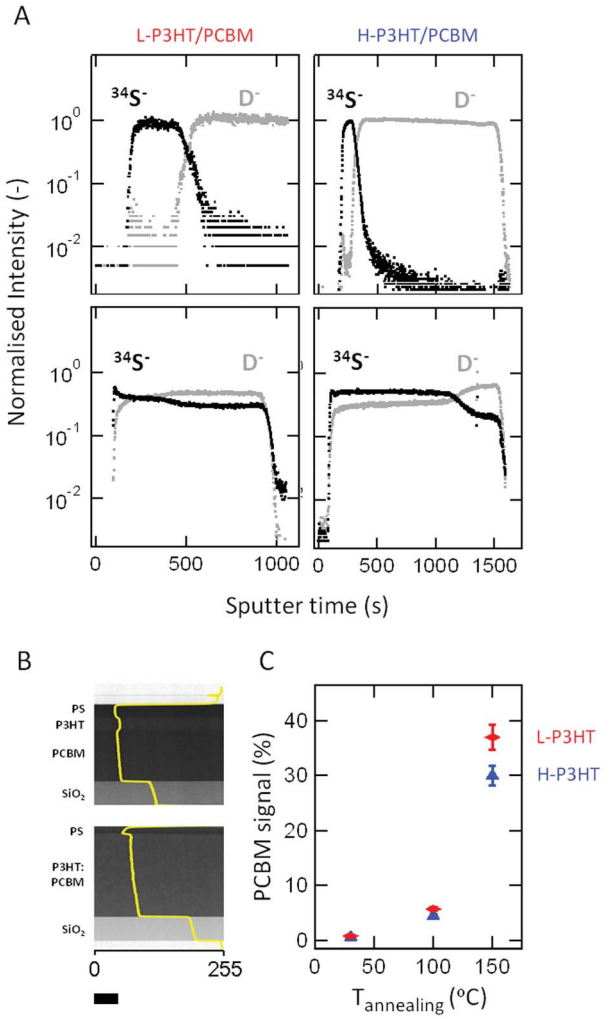

Fig. 2 Depth profile and cross-section analysis of P3HT/PCBM bilayers, as prepared and after annealing, performed by dynamic SIMS and HAADF STEM. (A) Depth profiles of pristine bilayers L-P3HT/PCBM (top left), H-P3HT/P3HT (top right) and annealed (150 °C, 30 s) bilayers L-P3HT/PCBM (bottom left) and H-P3HT/PCBM (bottom right). Sulphur trace (corresponding to P3HT) and deuterium trace (corresponding to D_5-PCBM) are shown in black and grey respectively. (B) Scanning transmission electron micrographs of H-P3HT/PCBM bilayers, pristine (top) and annealed (bottom). The integrated image intensity (yellow) is shown overlaid. The *x*-axis corresponds to 8-bit greyscale, where 0 = black and 255 = white. Intermediate values are the remaining 254 shades of grey. The scale bar represents 100 nm. Higher resolution versions of the images displayed can be found in Fig. S3.† The thicknesses observed here are in the range expected for such processing conditions. The orange lines added to the image are a guide for the eye, to aid identification of the interfaces (C) Quantity of interdiffused PCBM into (red diamonds) L-P3HT and (blue triangles) H-P3HT deduced from the d-SIMS data presented in (A) as a function of temperature. The quantity of intermixed PCBM is given as percent of signal relative to a PCBM reference.

comparison. In fact, PCBM is known to act as vitrifier for P3HT when they are deposited from a common solvent,[37] while the polymer very likely can more readily crystallise in the absence of the fullerene, as is the case for the neat P3HT films during the bilayer fabrication.

We hence set out to gain a better understanding of the microstructures of H-P3HT:PCBM and L-P3HT:PCBM blends and their corresponding H-P3HT/PCBM, L-P3HT/PCBM bilayers. As a simple probe of the microstructure of these systems (as prepared and annealed) we utilised UV-vis spectroscopy because the optical absorption of P3HT is very sensitive to changes in the local environment and molecular arrangement of the P3HT macromolecules, and can be interpreted using the Spano model of weakly interacting H-aggregates.[42] According to this model, the ratio of the 0–0/0–1 vibronic transitions (at ~595 and ~550 nm, respectively, see (Fig. 3)) can be related to the magnitude of aggregation and, therefore, intermolecular coupling within the system. In addition, the disordered polymer chains give rise to a higher energy, lower wavelength, λ, absorption (at $\lambda < 540$ nm).

Tellingly, considerable differences were observed between the spectra obtained for P3HT:PCBM thin films that were deposited from a common solvent (Fig. 3 – left panels) and P3HT/PCBM bilayers (Fig. 3 – right panels). The as-cast blend films featured noticeably larger contributions from the

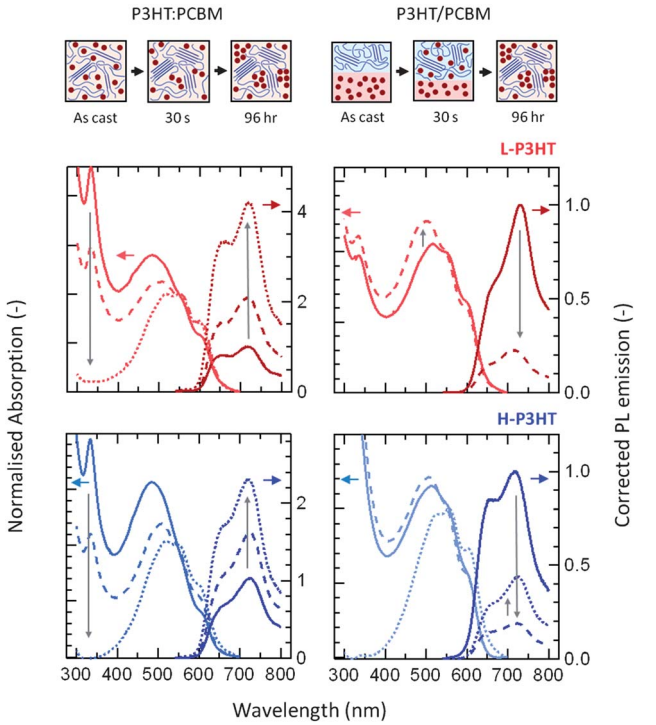

Fig. 3 Evolution of opto-electronic and structural properties of P3HT:PCBM and P3HT/PCBM systems with processing, thermal annealing and molecular weight. Top panel: schematics illustrating the structural evolution of P3HT:PCBM blends (left) and P3HT/PCBM bilayers (right) as deduced from the UV-vis and PL data presented in the two lower panels. The blend system exhibits the most intermixed structure. Annealing for 30 s enhances the fraction of polymer aggregates. Annealing for longer times additionally promotes the crystallisation of PCBM. The bilayer system, exhibits a higher fraction of aggregates initially; annealing for 30 s promotes interdiffusion of PCBM, disrupting some polymer aggregates. Annealing for 96 hours promotes macroscopic crystallisation of PCBM. Middle panel: UV-vis and PL spectra obtained for systems of L-P3HT:PCBM. Bottom panel: UV-vis and PL spectra of H-P3HT:PCBM binaries. A comparison is shown for all systems: pristine (*i.e.* as-prepared) (solid lines), and annealed at 150 °C for 30 s (dashed) and 96 hours (dotted). UV-vis absorption spectra were normalised to the 0–1 vibronic transition (~550 nm). Photoluminescence spectra have been corrected for the absorption at the excitation wavelength 520 nm and then normalised to the emission of the pristine sample.

absorption related to the non-aggregated (*i.e.* molecularly largely disordered) polymer fractions, when compared to that of the pristine bilayers (Fig. 3, solid lines). This is consistent with the fact that the as-cast blend films also exhibit a suppressed 0–0/0–1 absorption ratio – a further indication that the polymer chains are more poorly aggregated in these systems. These observations imply that in the as-cast P3HT:PCBM blends, the fullerene indeed acted as vitrifier, preventing molecular ordering in the polymer – as found previously, while in the pristine P3HT/PCBM bilayers – the polymer is relatively well aggregated as it could order in a reasonably unhindered manner leading to the enhanced 0–0/0–1 absorption feature. Note in addition, that for both the blend and bilayer systems, the L-P3HT showed a higher 0–0/0–1 absorption ratio when compared to the H-P3HT; we attribute this enhanced aggregation of L-P3HT to the differences in kinetics of ordering between the two different donor polymers, with the low molecular-weight material being able to order more readily. These observations appear to correlate with grazing incidence wide angle X-ray scattering (GIWAXS) (Fig. S1†), whereby the L-P3HT:PCBM blend exhibits more intense/sharper reflections corresponding to molecularly more ordered P3HT when compared to H-P3HT:PCBM blends. Upon short annealing (30 s/150 °C) the P3HT:PCBM blends showed a significant change in their optical absorption behaviour (Fig. 3 – left panels; dashed lines) independent of the molecular weight of the polymer. In both the L-P3HT and H-P3HT systems there is a noticeable increase in 0–0/0–1 absorption ratio with respect to the as-cast films. This is accompanied by a decrease in the higher-energy (lower wavelength) absorption, corresponding to a reduction of the disordered polymer fractions (Fig. 3). These observations are all consistent with the picture of the polymer aggregating upon annealing and, as a consequence, expelling at least a certain fraction of the PCBM molecules, as schematically depicted in Fig. 3, left panel. The latter picture is supported by the fact that annealing also leads to significantly enhanced photoluminescence (PL) (4× and 2× increase for L-P3HT and H-P3HT respectively), consistent with the two components phase separating, as schematically depicted in Fig. 3, top left panel.

Annealing of the P3HT:PCBM blends for a further 96 hours at 150 °C to drive the systems more towards their quasi-thermodynamic equilibrium state,[13] resulted in additional changes in their UV-vis absorption behaviour (dotted lines, Fig. 3, left panels). Firstly, the fullerene absorption around ~340 nm is greatly reduced during this additional annealing; this has been previously ascribed to the crystallisation of the PCBM into microscopically large crystals[13] that were observed in optical microscopy (Fig. S2†). We utilised scanning transmission X-ray microscopy (STXM) to confirm and quantify the reduced content of the fullerene within the polymer matrix yielding fullerene contents of ~5.2 and 7.1 wt% for H-P3HT and L-P3HT, respectively (Fig. S2†). For the blend films comprising H-P3HT:PCBM (Fig. 3, bottom panels), the 0–0 absorption transition became more pronounced upon this treatment while for the binary structures fabricated with L-P3HT (Fig. 3, middle panels) no further increase in the degree of aggregation was found, supporting the picture that the ordering of L-P3HT:PCBM blend films is kinetically less hindered due to the predominantly un-entangled nature of this short-chain P3HT.

In stark contrast to the blend films, L-P3HT/PCBM and H-P3HT/PCBM-bilayers showed a significant increase in their disordered absorption feature at low wavelengths already upon annealing for 30 s, accompanied by a small decrease in the relative 0–0 transition (Fig. 3 – right panel; dashed lines). This strongly suggests that interdiffusion of the PCBM molecules into the polymer layer disrupts the aggregated P3HT moieties, as previously postulated,[10] leading to this observed changes in the UV-vis spectra. In accord with the former observation is the fact that such short-annealed bilayers displayed – in strong disparity with the P3HT:PCBM blend systems – a five-fold *decrease* in PL when compared to the as-prepared bilayers (Fig. 3, right panels), concurrent with a higher degree of intermixing of the fullerene into the polymer. These observations appear to agree with initial GIWAXS measurements where changes in the diffraction are observed (Fig. 4). The latter is more pronounced in bilayers comprised of H-P3HT, possibly supporting that the diffusion of PCBM may disrupt the aggregation of P3HT for this molecular weight. The dependence of this effect on molecular weight is consistent with a previous report using lower molecular weight P3HT (M_w = 42.2k) where diffusion of PCBM did not strongly disrupt P3HT order.[15] Note, though, that in H-P3HT/PCBM systems prolonged annealing (96 hours/150 °C) resulted in an increase in the PL compared to the short-annealed system, suggestive of the components phase separating during this treatment.

It is clear from the UV-vis, PL spectroscopy data and complementary GIWAXS measurements that the two processing protocols discussed here lead to entirely different phase morphologies in the various P3HT:PCBM and P3HT/PCBM systems investigated here. As a consequence, the resulting architectures follow different solid-state structure developments upon further post-deposition treatment, such as annealing. It is

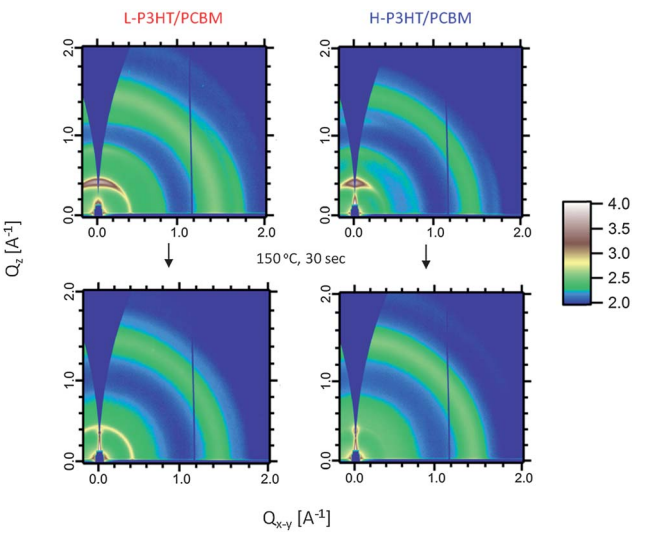

Fig. 4 Grazing incidence wide angle X-ray scattering patterns of pristine and annealed P3HT/PCBM bilayers. Left: L-P3HT/PCBM bilayers, pristine (top) and annealed at 150 °C for 30 s (bottom). Right: H-P3HT/PCBM bilayers, pristine (top) and annealed at 150 °C for 30 s (bottom).

therefore evident that the d-SIMS and TAS data presented in Fig. 1 and 2 address different microstructures and, hence, require greater understanding to be compared directly. Because the four systems – *i.e.* H-P3HT:PCBM, L-P3HT:PCBM, H-P3HT/PCBM, L-P3HT/PCBM – provide a range of different phase morphologies, it is however also clear that we obtain a means to elucidate how aggregation, phase separation and intermixing affect the opto-electronic processes. Indeed, the largest portions of intermixed phase are found in the as-cast H-P3HT:PCBM blend films and H-P3HT/PCBM bilayer structures that were annealed for 30 s at 150 °C, while prolonged annealing of H-P3HT:PCBM leads to a system that comprises a considerable fraction of relatively pure phases. A well-defined two-phase system is obviously provided by the as-prepared bilayers (see Fig. 3 for schematic illustrations of the various microstructures).

When comparing the binaries of highest/lowest intermixing, it is intriguing to find that the highest charge generation deduced from the ΔOD measured in TAS is found for the most intermixed structures: *i.e.* as-cast H-P3HT:PCBM blend films and short-annealed H-P3HT/PCBM bilayers (Fig. 5). The stronger the systems phase separate, *i.e.* driven by annealing of P3HT:PCBM blend thin-films, the lower the measured ΔOD; as-prepared bilayers feature the lowest charge generation.

We now turn to considering the difference in the transient absorption signal amplitudes of the various systems. The question that arises here is why we see such differences in the ΔOD for the various P3HT:PCBM samples; whether the difference originates from variation in exciton quenching at the donor/acceptor interface or, rather, whether the dissociation of charge transfer states into free photogenerated charge carriers (geminate recombination) is influencing the observed trend. The summarised ΔOD signal intensities are shown in Table S1.† They are normalized for variations in the density of absorbed photons due to variations in film optical density at the excitation wavelength, ΔOD/OD and variations in PL quenching (PLQ) ΔOD/PLQ observed between the blend films. It is apparent that for the as cast blends and annealed bilayer films, these changes in ΔOD signal intensities, and therefore yield of dissociated polarons, do not correlate with the variation in PL quenching observed between the films. As such, these variations in polaron yields cannot be assigned primarily to changes in the efficiency of exciton dissociation. Rather, as we have concluded previously for other materials systems,[40,43] the observation in variation of the polaron yield is more reasonably assigned primarily to variations in geminate recombination losses on the pico-nanosecond timescales and, thus, to the variations in the efficiency of dissociation of interfacial charge transfer (CT) states into free charges.

Our observations give clear guidelines on how to optimise the photo-physical processes leading to charge generation in OPV systems by providing for a certain degree of miscibility between the donor and acceptor material. Indeed, our results highlight the importance of an intermixed phase in the processes of exciton quenching and charge generation in these systems. It is important to underline, however, that it seems critical that these intermixed phases co-exist with relatively phase-pure regions (*e.g.* crystalline P3HT moieties), in agreement with recent findings.[44] In fact, full miscibility, *i.e.* formation of a one-phase system comprised of a solid solution appears not to be desirable.[15,17,45] Structures comprising low PCBM fraction, where rather complete intermixing can be expected, consistently showed lower charge generation independent of the processing protocols selected. This is because geminate recombination processes very likely will limit charge generation and device performance.[39] On the contrary, for binaries comprising 50 wt% of the fullerene where some fullerene aggregation can be expected, higher ΔOD values were measured. The optimum amount of intermixing still needs to be quantified and may vary from system to system; clearly, it will also depend on the lateral length scales of the phases created.

In addition, it is evident that compromises need to be reached between optimising excited state quenching, charge generation (which according to our study are favoured by phase morphologies comprising considerable fractions of an intermixed phase along with phase-pure regions) and the subsequent processes resulting in best device performance. Indeed, highest solar cell efficiencies for P3HT:PCBM systems comprising 50 wt% PCBM are obtained after annealing of solution-cast active layers – that is in a system of lower excited state quenching where larger quantities of relatively phase-pure domains of the two components can develop. Our findings moreover should assist in designing new OPV materials and aid in advancing reliable processing protocols without the need of time-consuming trial-and-error procedures.

In conclusion, our observations show the significance and intricacy of the processes leading to the structural evolution of BHJs, including: diffusion, phase separation and frequently, the interplay between crystallisation and vitrification. These processes have been shown to have a significant effect on the photo-physical processes leading to polaron formation and are believed to be strongly affected by the degree of geminate recombination which acts as a loss mechanism, tuneable by the processing route employed. Furthermore it is proposed that the

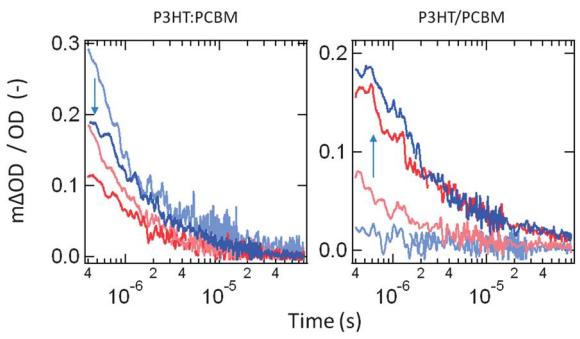

Fig. 5 Transient absorption signals: phase purity dependence of dissociated polaron yield (ΔOD) of L-P3HT (red) and H-P3HT (blue) systems for P3HT:PCBM blends (left) and P3HT/PCBM bilayer (right) systems, following pulsed laser excitation at 520 nm at an excitation intensity of 2 μJ cm^{-2} and a probe wavelength of 980 nm. Data for pristine samples are shown in lighter shades. Annealed samples are shown in darker shades. The bilayer samples were annealed at 150 °C for 30 s, corresponding to the most mixed state of the bilayers. The blend samples were annealed at 150 °C for 96 hours, corresponding to the most phase pure state of the blends.

molecular weight of the polymer can be used as a tool to optimise the microstructure not only by the chain extended/semi-crystalline nature of L-P3HT and H-P3HT, respectively, but also because of the difference in rate of ordering seen between the two materials. Consideration of the sensitive interplay of structural processes is of paramount importance to realise a microstructure that allows formation of a certain fraction of intermixed phase. Thereby, the dependence of these processes on the initially prepared microstructure needs to be taken into account. Inducing more crystalline structures, for instance (as realised here in pristine bilayers) reduces not only interdiffusion of the two components but also limits our means to readily induce partial phase separation. Annealing can lead to higher intermixed structures, but in other cases to more pronounced phase segregation depending on the initial solid-state microstructure, phase morphology and the 'intrinsic' miscibility of the system. Note in this context that changes in microstructure can also influence other properties such as the ionisation potential of the material. Clearly, intimate knowledge of the chemical interaction potential and crystallisation behaviour between the two components will thus be a highly useful tool to predict the thermodynamically more favoured state. Such considerations can be expected to be even more relevant for systems that have a low tendency to molecularly order, such as some of the more complex donor/acceptor polymers or many of the newly developed electron accepting materials where the driving force to crystallise and, hence, phase separation is dominated by the mutual miscibility of the key components. Relatively straight-forward techniques, such as PL and UV-vis spectroscopy, thereby provide highly valuable insight in the structural features of these systems.

Materials and methods

Materials

The two molecular weights of P3HT, L-P3HT (M_n = 5.1 kg mol^{-1}, M_w = 7.2 kg mol^{-1}, RR > 95% by integration of the methylene region not correcting for end-group effect) and H-P3HT (M_n = 70 kg mol^{-1}, M_w = 135 kg mol^{-1}, RR = 99%) were prepared by the Grignard metathesis polymerisation as previously reported.[46] L-P3HT and H-P3HT were prepared using a reaction temperatures of 0 °C and 55 °C and catalyst ratios of 1 mol% and 0.15 mol% of Ni(dppp)Cl_2 respectively. The polymers were purified by Soxhlet extraction with methanol and acetone. The remaining polymer was dissolved in chloroform, filtered and precipitated into methanol. Number-average (M_n) and weight-average (M_w) molecular weights were determined by Agilent Technologies 1200 series GPC running in chlorobenzene at 80 °C, using two PL mixed B columns in series, and calibrated against narrow polydispersity polystyrene standards. PCBM (>99.5% purity) was purchased from Solenne, BV, all materials were used as received.

Solutions

Solutions were prepared from chlorobenzene, by dissolving the solute at 80 °C with stirring. All of the substrates were washed sequentially in: deionised water (with 0.1% detergent); acetone and iso-propanol for 15 min each with ultrasonication, followed by blow-drying with nitrogen.

Blend films

Blend films were fabricated by dissolving the polymer and fullerene at appropriate ratios, so the total solute concentration was 2% (w/v) in chlorobenzene. These solutions were then spin cast at 1200 rpm onto pre-cleaned glass substrates and dried under vacuum for 24 hours. Thermal annealing was carried out in a vacuum oven for 30 s (short annealed) and 96 hours (long annealed) in the dark.

Bilayers

Bilayers were fabricated by spin casting PCBM 3% (w/v) at 800 rpm for 60 s onto a first substrate (glass for UV-vis, PL and TAS or SiO_2 for d-SIMS, GIWAXS samples were made on Si substrates while those for STXM were made on PSS-coated glass substrates). P3HT was then spin cast 2% (w/v) at 1200 rpm for 60 s onto an SiO_2 substrate. The two bilayer component layers were left under vacuum for 48 hours to aid removal of residual solvent. The P3HT layer was then delaminated using a 5% (v/v) solution of HF in water and subsequently floated onto a bath of deionised water. The free-floating P3HT films were then picked up by PCBM coated substrate. The bilayers were then placed under vacuum for 12 hours the aid lamination. Thermal annealing was then carried out for 30 s (short annealed) and 96 hours (long annealed). Samples prepared for d-SIMS and TEM had a subsequent layer of PS floated on top to aid intensity and sputter rate calibration of the d-SIMS. Ongoing work has demonstrated good agreement with the elemental and larger fragment signals, implying that, in this case, elemental signals provide a good tool for probing molecular vertical composition.

UV-vis spectroscopy

UV-vis spectroscopy was carried out using a Perkin-Elmer Lambda 35, 1 nm increment at 1280 nm min^{-1}.

Steady state photoluminescence (PL)

Steady state photoluminescence (PL) utilised a Horiba Spex Fluormax-1 spectrofluorometer with slit widths of 5 nm and an integration time of 0.2 s. All samples were excited at 520 nm and emission intensity was corrected for differences in optical absorption.

Transient absorption

Transient absorption decays were measured by exciting the sample film, under a nitrogen (and oxygen) atmosphere, pumped with a Nd:YAG laser (Lambda Photometrics). The excitation wavelength used was 520 nm, with a pump intensity of 2 μJ cm^{-2} and a repetition frequency of 20 Hz. A 100 W quartz halogen lamp (Bentham, IL 1) with a stabilised power supply (Bentham, 605) was used as the probe light source (at 980 nm). The probe light passing through the sample film was detected with a silicon photodiode (Hamamatsu Photonics, S1722-01).

The signal from the photodiode was pre-amplified and sent to the main amplification system with an electronic band-pass filter (Costronics Electronics). The amplified signal was collected with a digital oscilloscope (Tektronics, TDS220), which was synchronised with a trigger signal of the pump laser pulse from a photodiode (Thorlabs Inc., DET210). To reduce stray light, scattered light and sample emission, two monochromators and appropriate optical cut-off filters were placed before and after the sample.

Dynamic secondary ion mass spectrometry (SIMS)

An Ion TOF 5 SIMS was used to measure depth profiles of bilayer samples. All samples were sputtered using a 1 keV Cs^+ (~75 nA) beam across a 250 × 250 μm square. Analysis was carried out using a Bi_3^+ (~1 pA) beam over the central 50 × 50 μm region of the sputter crater with charge compensation and negative ions were collected. We note the use of time axis in the depth profiles is due to the large differences (~4×) in sputter rates of the polymer and fullerene. In addition the sputter rate is non-linear with composition (manuscript in preparation) making an accurate depth rescale, whilst preserving interface information difficult. In addition the differences in polymer layer thickness appear accentuated due to differing time scale of the *x*-axis, plotted to allow clearer comparison of all samples and possible difference in sputter rate of the two polymers.

Grazing incidence wide angle X-ray scattering (GIWAXS)

Grazing incidence wide angle X-ray scattering (GIWAXS) was carried out at Beamline 7.3.3. of the Advanced Light Source[47] using a Dectris Pilatus 1M photon counting detector. Samples were measured at an incident angle of ~0.13°, above the critical angle so the X-ray beam penetrated to the substrate. The photon energy used for GIWAXS was 10 keV. Air scatter which provides a background signal was reduced using helium gas.

Scanning transmission X-ray microscopy (STXM)

Scanning transmission X-ray microscopy (STXM) was conducted at Beamline 5.3.2.2 of the ALS.[48] During measurement, the chamber was filled with 1/3 ATM He. Miscibility values of long annealed samples were determined from absorbance measurements following previously described procedures.[49] In order to gain a quantitative measure of fullerene solubilised in the polymer at the local thermodynamic equilibrium, samples must be annealed for significantly long times (~96 hours) to ensure the system has reached equilibrium condition.

Transmission electron microscopy (TEM)

To characterise the morphology and thickness of the polymer layers an electron transparent cross-section of the polymer films on Si/SiO_2 was prepared using a focussed ion beam (FIB) dual beam system (FEI Helios NanoLab). Initially, the surface of the polymer films was coated with a thin (~15 nm) chromium layer to provide a conductive surface. A platinum strap was then deposited onto the surface to protect surface features. The region surrounding the Pt strap was then milled using 30 kV Ga^+ ions creating a lamella. The lamella, when extracted and attached to a TEM grid, was thinned using the Ga^+ beam, operated at successively lower accelerating voltages and beam currents. The prepared specimen was examined using an FEI Titan 80-300 TEM operated at 300 kV in STEM mode, with incoherently scattered electrons collected using a high angle annular dark field (HAADF) detector to form the images. The brightness and contrast of the HAADF detector are optimised to provide maximum contrast between the polymer layers. Since the cross-section was taken parallel to a cleaved crystalline edge of the Si/SiO_2 substrate, the diffraction pattern produced from the substrate can be used to tilt the lamella so that the substrate surface is parallel to the electron beam, ensuring the interfaces within the polymer films are also parallel to the electron beam.

Acknowledgements

We are very grateful to the UK's Engineering and Physical Sciences Research Council (EPSRC) for financial support *via* the Doctoral Training Centre in Plastic Electronics EP/G037515/1 (PW, NS, JdM and JB), the EPSRC platform grant EP/G060738/1 (NS) and (JG and SH) the Doctoral Training Account; Imperial College SIMS facility is supported by EP/H006060/1. We furthermore acknowledge the ACS Petroleum Fund (New Directions Grant). NS is also supported by a European Research Council (ERC) Starting Independent Researcher Fellowship under the grant agreement no. 279587. X-ray characterization and analysis by JT and HA were supported by DOE, OS, BES, MSE (DE-FG02-98ER45737). Data were acquired at beamlines 5.3.2.2 and 7.3.3 of the ALS, which is supported by DOE (DE-AC02-05CH1123). Thanks are given to David Kilcoyne at Beamline 5.3.2.2 and Eric Schaible at Beamline 7.3.3 for assistance with data acquisition. Eliot Gann is also acknowledged for assistance with GIWAXS analysis. JB holds an Industrial Fellowship with the Royal Commission for the Exhibition of 1851. JdM acknowledges financial support under the Royal Society Industry Fellowship scheme.

References

1 M. A. Green, K. Emery, Y. Hishikawa, W. Warta and E. D. Dunlop, *Prog. Photovoltaics*, 2012, **20**, 12–20.
2 Y. Liang, Z. Xu, J. Xia, S.-T. Tsai, Y. Wu, G. Li, C. Ray and L. Yu, *Adv. Mater.*, 2010, **22**, E135–E138.
3 N. Blouin, A. Michaud and M. Leclerc, *Adv. Mater.*, 2007, **19**, 2295–2300.
4 T.-Y. Chu, S. Alem, P. G. Verly, S. Wakim, J. Lu, Y. Tao, S. Beaupré, M. Leclerc, F. Bélanger, D. Désilets, S. Rodman, D. Waller and R. Gaudiana, *Appl. Phys. Lett.*, 2009, **95**, 063304.
5 M. C. Scharber, M. Koppe, J. Gao, F. Cordella, M. A. Loi, P. Denk, M. Morana, H.-J. Egelhaaf, K. Forberich, G. Dennler, R. Gaudiana, D. Waller, Z. Zhu, X. Shi and C. J. Brabec, *Adv. Mater.*, 2010, **22**, 367–370.
6 H. Bronstein, Z. Chen, R. S. Ashraf, W. Zhang, J. Du, J. R. Durrant, P. S. Tuladhar, K. Song, S. E. Watkins, Y. Geerts, M. M. Wienk, R. a. J. Janssen, T. Anthopoulos,

H. Sirringhaus, M. Heeney and I. McCulloch, *J. Am. Chem. Soc.*, 2011, **133**, 3272–3275.
7 J. Hou, H.-Y. Chen, S. Zhang, G. Li and Y. Yang, *J. Am. Chem. Soc.*, 2008, **130**, 16144–16145.
8 H. Lu, B. Akgun and T. P. Russell, *Adv. Energy Mater.*, 2011, **1**, 870–878.
9 M. Pfannmöller, H. Flügge, G. Benner, I. Wacker, C. Sommer, M. Hanselmann, S. Schmale, H. Schmidt, F. a. Hamprecht, T. Rabe, W. Kowalsky and R. R. Schröder, *Nano Lett.*, 2011, **11**, 3099–3107.
10 N. D. Treat, M. A. Brady, G. Smith, M. F. Toney, E. J. Kramer, C. J. Hawker and M. L. Chabinyc, *Adv. Energy Mater.*, 2011, **1**, 82–89.
11 N. D. Treat, A. Varotto, C. J. Takacs, N. Batara, M. Al-Hashimi, M. J. Heeney, A. J. Heeger, F. Wudl, C. J. Hawker and M. L. Chabinyc, *J. Am. Chem. Soc.*, 2012, **134**, 15869–15879.
12 B. A. Collins, E. Gann, L. Guignard, X. He, C. R. McNeill and H. Ade, *J. Phys. Chem. Lett.*, 2010, **1**, 3160–3166.
13 B. Watts, W. J. Belcher, L. Thomsen, H. Ade and P. C. Dastoor, *Macromolecules*, 2009, **42**, 8392–8397.
14 H. W. Ro, B. Akgun, B. T. O. Connor, M. Hammond, R. J. Kline, C. R. Snyder, S. K. Satija, A. L. Ayzner, M. F. Toney, C. L. Soles and D. M. Delongchamp, *Macromolecules*, 2012, **45**, 6587–6599.
15 D. Chen, F. Liu, C. Wang, A. Nakahara and T. P. Russell, *Nano Lett.*, 2011, **11**, 2071–2078.
16 W. Yin and M. Dadmun, *ACS Nano*, 2011, **5**, 4756–4768.
17 B. A. Collins, Z. Li, J. R. Tumbleston, E. Gann, C. R. McNeill and H. Ade, *Adv. Energy Mater.*, 2013, **3**, 65–74.
18 J. A. Bartelt, Z. M. Beiley, E. T. Hoke, W. R. Mateker, J. D. Douglas, B. A. Collins, J. R. Tumbleston, K. R. Graham, A. Amassian, H. Ade, J. M. J. Fréchet, M. F. Toney and M. D. McGehee, *Adv. Energy Mater.*, 2013, **3**, 364–374.
19 W. Chen, T. Xu, F. He, W. Wang, C. Wang, J. Strzalka, Y. Liu, J. Wen, D. J. Miller, J. Chen, K. Hong, L. Yu and S. B. Darling, *Nano Lett.*, 2011, **11**, 3707–3713.
20 D. M. Delongchamp, R. J. Kline and A. Herzing, *Energy Environ. Sci.*, 2012, **5**, 5980–5993.
21 W. Chen, M. P. Nikiforov and S. Darling, *Energy Environ. Sci.*, 2012, **5**, 8045–8074.
22 B. A. Collins, J. R. Tumbleston and H. Ade, *J. Phys. Chem. Lett.*, 2011, **2**, 3135–3145.
23 K. Vakhshouri, D. R. Kozub, C. Wang, A. Salleo and E. D. Gomez, *Phys. Rev. Lett.*, 2012, **108**, 026601.
24 H. Hoppe and N. S. Sariciftci, *J. Mater. Res.*, 2004, **19**, 1924–1945.
25 J. Piris, T. E. Dykstra, A. A. Bakulin, P. H. M. Van Loosdrecht, W. Knulst, M. T. Trinh, J. M. Schins and L. D. A. Siebbeles, *J. Phys. Chem. C*, 2009, **113**, 14500–14506.
26 I. A. Howard, R. Mauer, M. Meister and F. Laquai, *J. Am. Chem. Soc.*, 2010, **132**, 14866–14876.
27 F. Etzold, I. A. Howard, R. Mauer, M. Meister, T.-D. Kim, K.-S. Lee, N. S. Baek and F. Laquai, *J. Am. Chem. Soc.*, 2011, **133**, 9469–9479.
28 M. Tong, N. E. Coates, D. Moses and A. J. Heeger, *Phys. Rev. B: Condens. Matter Mater. Phys.*, 2010, **81**, 125210.
29 G. Grancini, M. Maiuri, D. Fazzi, A. Petrozza, H.-J. Egelhaaf, D. Brida, G. Cerullo and G. Lanzani, *Nat. Mater.*, 2012, **11**, 1–5.
30 P. A. Troshin, H. Hoppe, J. Renz, M. Egginger, J. Y. Mayorova, A. E. Goryachev, A. S. Peregudov, R. N. Lyubovskaya, G. Gobsch, N. S. Sariciftci and V. F. Razumov, *Adv. Funct. Mater.*, 2009, **19**, 779–788.
31 P. Schilinsky, U. Asawapirom, U. Scherf, M. Biele and C. J. Brabec, *Chem. Mater.*, 2005, **17**, 2175–2180.
32 P. J. Flory and J. Rehner, *J. Chem. Phys.*, 1943, **11**, 521–526.
33 O. G. Reid, J. A. Nekuda Malik, G. Latini, S. Dayal, N. Kopidakis, C. Silva, N. Stingelin and G. Rumbles, *J. Polym. Sci., Part B: Polym. Phys.*, 2012, **50**, 27–37.
34 M. Brinkmann and P. Rannou, *Adv. Funct. Mater.*, 2007, **17**, 101–108.
35 R. J. Kline, M. D. McGehee, E. N. Kadnikova, J. Liu and J. M. J. Fréchet, *Adv. Mater.*, 2003, **15**, 1519–1522.
36 A. J. Ferguson, N. Kopidakis, S. E. Shaheen and G. Rumbles, *J. Phys. Chem. C*, 2011, **115**, 23134–23148.
37 C. Müller, T. A. M. Ferenczi, M. Campoy-Quiles, J. M. Frost, D. D. C. Bradley, P. Smith, N. Stingelin-Stutzmann and J. Nelson, *Adv. Mater.*, 2008, **20**, 3510–3515.
38 A. F. Nogueria, I. Montanari, J. Nelson, J. R. Durrant, C. Winder, N. S. Sariciftci and C. Brabec, *J. Phys. Chem. B*, 2003, **107**, 1567–1573.
39 T. M. Clarke, A. Ballantyne, S. Shoaee, Y. W. Soon, W. Duffy, M. Heeney, I. McCulloch, J. Nelson and J. R. Durrant, *Adv. Mater.*, 2010, **22**, 5287–5291.
40 H. Ohkita, S. Cook, Y. Astuti, W. Duffy, S. Tierney, W. Zhang, M. Heeney, I. McCulloch, J. Nelson, D. D. C. Bradley and J. R. Durrant, *J. Am. Chem. Soc.*, 2008, **130**, 3030–3042.
41 F. C. Jamieson, E. B. Domingo, T. McCarthy-Ward, M. Heeney, N. Stingelin and J. R. Durrant, *Chem. Sci.*, 2012, **3**, 485–492.
42 (*a*) J. Clark, C. Silva, R. H. Friend and F. C. Spano, *Phys. Rev. Lett.*, 2007, **98**, 206406; (*b*) J. Clark, J.-F. Chang, F. C. Spano, R. H. Friend and C. Silva, *Appl. Phys. Lett.*, 2009, **94**, 163303–163306.
43 S. Shoaee, T. M. Clark, C. Huang, S. Barlow, S. R. Marder, M. Heeney, I. McCulloch and J. R. Durrant, *J. Am. Chem. Soc.*, 2010, **132**, 12919–12926.
44 S. Shoaee, S. Subramaniyan, H. Xin, C. Keiderling, P. S. Tuladhar, F. C. Jamieson, S. A. Jenekhe and J. R. Durrant, *Adv. Funct. Mater.*, 2013, **23**, 3286–3298.
45 B. A. Collins, Z. Li, C. R. McNeill and H. Ade, *Macromolecules*, 2011, **44**, 9747–9751.
46 R. S. Loewe, P. C. Ewbank, J. Liu, L. Zhai and R. D. McCullough, *Macromolecules*, 2001, **34**, 4324.
47 A. Hexemer, W. Bras, J. Glossinger, E. Schaible, E. Gann, R. Kirian, A. MacDowell, M. Church, B. Rude and H. Padmore, *J. Phys.: Conf. Ser.*, 2010, **247**, 012007.
48 A. L. D. Kilcoyne, T. Tyliszczak, W. F. Steele, S. Fakra, P. Hitchcock, K. Franck, E. Anderson, B. Harteneck, E. G. Rightor, G. E. Mitchell, A. P. Hitchcock, L. Yang, T. Warwick and H. Ade, *J. Synchrotron Radiat.*, 2003, **10**, 125.
49 B. A. Collins and H. Ade, *J. Electron Spectrosc. Relat. Phenom.*, 2012, **185**, 119.

